

## Avalanches and Self-Organization in Cellular Magnetic-Domain Patterns

K. L. Babcock<sup>(a)</sup> and R. M. Westervelt

*Division of Applied Sciences and Department of Physics, Harvard University, Cambridge, Massachusetts 02138*  
(Received 3 November 1989)

We report observations of avalanchelike, topological rearrangements of cellular domain patterns in magnetic garnet films. Over significant intervals in applied magnetic field and cell density, the patterns self-organize into barely stable states. Small field increments trigger avalanches of cell destruction that span more than 2 orders of magnitude in size and lifetime.

PACS numbers: 75.60.-d, 05.40.+j, 64.60.Ht

A number of model systems with many spatial degrees of freedom and dissipative dynamics have recently been shown to self-organize into states which are barely stable. Examples include driven chains of nonlinear oscillators,<sup>1</sup> models of earthquake dynamics,<sup>2</sup> cellular automata that approximate the dynamics of sandpiles,<sup>3,4</sup> and models of domain walls in ferromagnetic films.<sup>5</sup> Perturbations destabilize the barely stable states, producing dynamical reorganizations which can occur on a wide range of time scales. The framework of self-organized criticality<sup>3,6</sup> has been proposed as a mechanism underlying such systems, and as a possible explanation for the  $1/f$  noise produced by many naturally occurring dynamic phenomena.<sup>7</sup> However, there have been few experimental demonstrations of these ideas to date.<sup>8</sup>

In this Letter, we describe observations of self-organizing dynamics in two-dimensional cellular magnetic-domain patterns. As described in detail elsewhere,<sup>9,10</sup> cellular domain patterns coarsen (reduce their cell density) in response to an increasing external mag-

netic bias field  $H_B$ . For fixed bias  $H_B$ , a pattern settles into a stationary configuration. When destabilized by subsequent increments in  $H_B$ , the pattern undergoes a sequence of topological changes that propagate via a domino effect until a new stationary configuration is reached. An example of such a topological avalanche is shown in the sequence of photographs in Fig. 1. Frame 1(a) shows the originally stationary pattern, comprised of segments of stripe domains (thin black lines) connected at threefold vertices and at small, fivefold-symmetric domain structures that contain trapped magnetic bubbles; five of these *pentagonal bubble traps* are visible in 1(a). This stationary pattern was destabilized by a small bias increment; the bias  $H_B$  was then held fixed. As shown in 1(b), a "knot" of high cell density contracts, pulled in by the stripe segments bounding the shaded central cell. The concentration of reversed magnetization in the knot produces a local field large enough to force the three adjoining bubble traps to collapse,<sup>9,11</sup> leaving the configuration 1(c). The resulting changes in

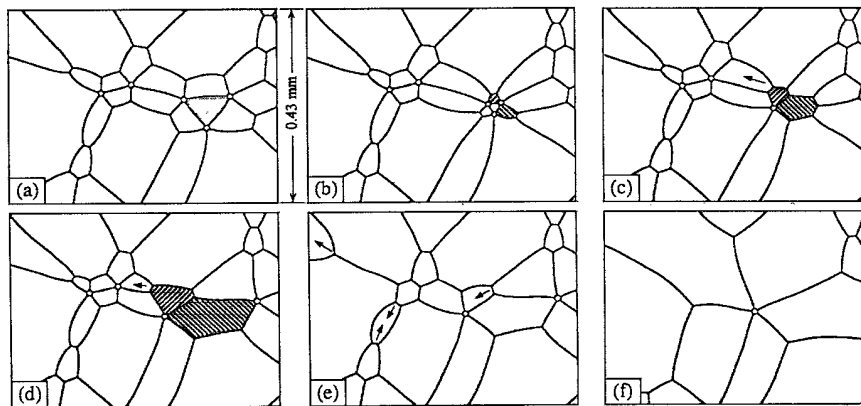


FIG. 1. Digitized photographs showing a topological avalanche triggered by a bias increment of 0.5 Oe; the bias was then held fixed at 89 Oe. White (black) regions correspond to up (down) magnetization. In (a), the central cell (shaded) surrounded by three bubble traps begins to contract. Between (b) and (c), all three bubble traps are destabilized and collapse, resulting in the configuration shown in (c). Hatching relates corresponding cells in (b), (c), and (d). Domain motion shown by the arrow encroaches on another knot, as shown in (d). The elimination of several cells occurs between (d) and (e), leaving a contracting four-sided cell, a vertex (upper left) moving toward yet another group of cells, and a contracting five-sided cell. After more cells vanished, the stationary state in (f) was reached 45 sec after the initial configuration was destabilized. A total of nineteen cells were eliminated within the field of view.

local topology destabilize the pattern, leading to cell-wall motion followed by the destruction of more cells. This process repeats, as illustrated in the remaining photographs of Fig. 1; see the caption for details. This avalanche lasted 45 sec and reduced the cell density by 56% within the field of view, which covers  $\sim 0.1\%$  of the usable area of the garnet film. An important feature of these avalanches is that the stationary patterns produced are barely stable, and additional small increments in applied field trigger new avalanches. The patterns thus self-organize into barely stable states.

These experiments focused on a bismuth-substituted iron-garnet film designed for use in magneto-optic devices.<sup>12</sup> The film has bulk magnetization  $4\pi M = 190$  G, thickness  $7.8 \mu\text{m}$ , Curie point  $T_{\text{Cur}} = 170^\circ\text{C}$ , and strong uniaxial magnetic anisotropy with easy axis perpendicular to the film plane. The anisotropy supports vertical domain walls that separate "up" and "down" domains comprised of magnetization aligned with and opposite to  $H_B$ , respectively.<sup>13</sup> The domain walls are narrow ( $\sim 0.1 \mu\text{m}$ ) compared to the domain sizes ( $\sim 10 \mu\text{m}$ ), and have an effective surface energy  $\sigma_w = 0.23 \text{ erg/cm}^2$ . The essentially two-dimensional patterns evolve by the lateral translation of the domain walls. In-depth discussions of the structure and energetics of cellular domain patterns are given in Refs. 9–11. We observed the domains with optical microscopy using the Faraday rotation of transmitted polarized light to provide contrast between up and down domains. Figure 1 is a digitized, high-contrast photograph, with white (black) areas corresponding to up (down) magnetization. Cellular patterns were produced from disordered "seas" of magnetic bubbles by aligning the bias field  $H_B$  with the bubble magnetization and increasing its magnitude to coarsen the pattern.<sup>9,10</sup> We have also observed domain avalanches qualitatively identical to those described here in three other device-quality garnet films.

For the data presented here, an ac-field component of frequency 40 Hz and amplitude 7.0 Oe was applied in addition to the dc bias to minimize the effects of coercive friction.<sup>13</sup> Without an ac field, the domains tend to stick, and domain-wall motion proceeds as a series of rapid jumps in position. For sufficiently large ac fields, avalanches are triggered by very small increments in bias field ( $\Delta H_B < 0.1$  Oe), and the domain motion is smooth and apparently viscous, with velocities typically  $< 100 \mu\text{m/sec}$ .<sup>9</sup> The results reported here rely on the smooth domain motion and the absence of sticking with an ac field.

Avalanches occur in the high-tension bias regime  $H_{\text{RI}} < H_B < H_5$ , where  $H_{\text{RI}} = 83.5$  Oe is the run-in field at which isolated stripe domains run in along their length to form bubbles or disappear into the edge of the sample,<sup>13</sup> and  $H_5 = 98.5$  Oe is the maximum field in which isolated pentagonal bubble traps are stable.<sup>9,11</sup> In this regime, domain motion following a change in bias field is driven by an imbalance between the effective tensions in

the stripe domains which form the cell walls. As in other cellular systems driven by cell-wall tension, cells with fewer than six sides tend to shrink and sometimes vanish.<sup>14</sup> However, the topological evolution of domain patterns is obstructed by small pentagonal bubble traps which resist elimination in local fields up to  $H_5$ .<sup>9,11</sup> Domain patterns in the high-tension regime are thus nonequilibrium, metastable states.<sup>9,10</sup>

Throughout the high-tension regime, cellular domain patterns are barely stable: Avalanches are triggered by bias increments as small as  $\Delta H_B = 0.1$  Oe. A bias increment typically triggers a number of independent avalanches, where the number grows with increment size. The dynamics of these domain patterns are self-organizing: Once the pattern settles into a stationary configuration, it is again susceptible to further avalanches for very small increments in  $H_B$ . This behavior is independent of the value of  $H_B$  or the size of the previous increment.

Domain avalanches occur as a series of separate events in which individual pentagonal bubble traps and other cells are destroyed, connected by intervening periods of cell-wall motion. The local magnetic field in the pattern varies spatially due to the stray demagnetization field from areas of down magnetization, and is largest in regions with a high concentration of cell walls. Thus bubble traps collapse first in locations with a high concentration of cell walls,<sup>11</sup> as shown in Fig. 1. Each destruction of a bubble trap destabilizes the pattern, and creates cell-wall motion, which increases the cell-wall density and local magnetic field in other parts of the pattern. This in turn can lead to the destruction of more cells, creating an avalanche.

A convenient measure of avalanche "size"  $s$  is the total number of cells eliminated by a given avalanche. In our experiments, avalanches proceed slowly enough that the eliminated cells can be counted by eye. An unambiguous measure of the avalanche lifetime  $T$  is given by the time between the first topological change and the cessation of domain motion. A delay up to several seconds occurs between the time of the bias increment and the first topological change; for example, the knot in Fig. 1(a) contracts slowly before the first bubble traps collapse. This delay is due simply to the slow speed of the domain walls in cellular patterns. In some cases, the pattern is apparently static immediately after an increment, followed by a smooth acceleration of domain walls toward the first cell elimination.

We determined the distributions of avalanche size and lifetime within the bias interval  $87 \text{ Oe} < H_B < 89 \text{ Oe}$ , entirely within the high-tension regime. Over this interval, the average cell density drops by  $\sim 40\%$ .<sup>10</sup> Avalanche statistics were compiled as follows: (i) The bubble seas were coarsened by gradually increasing  $H_B$  from zero to 87 Oe;  $H_B$  was then held fixed while the patterns settled. (ii) An increment  $\Delta H_B = 0.5$  Oe was applied, and the resulting avalanche sizes and lifetimes were tal-

lied as described above. Process (ii) was repeated four times, until  $H_B$  reached 89 Oe. Data were accumulated by repeating steps (i) and (ii). The 0.5-Oe bias increment was chosen because it triggered enough independent avalanches to speed data accumulation, while rarely producing "compound" avalanches formed by the collision of two avalanches triggered at separate locations. On average 7.8 avalanches were triggered per bias increment within the 10.8-mm<sup>2</sup> field of view, an area  $\sim 50$  times larger than the frames shown in Fig. 1.

Figure 2(a) is a plot of the sizes versus lifetimes observed for 1105 avalanches. The average size was  $\langle s \rangle = 8.5$  cells with a standard deviation of 10.6 cells, and the average lifetime was  $\langle T \rangle = 18.4 \pm 22.0$  sec. As shown,  $s$  and  $T$  are linearly correlated; the straight line in Fig. 2(a) is an unweighted fit to the data  $s = 0.5 + (0.43 \text{ sec}^{-1})T$ . The scatter in lifetime for a given size arises from variations in domain velocity, and because avalanches in which an entire knot collapses, eliminating several cells at once, tend to be of shorter duration than those in which cells are eliminated sequentially. Histograms of the avalanche lifetime and size are shown in Figs. 2(b) and 2(c). These distributions peak for small  $s$  and  $T$ , and have long tails spanning over two decades in both size and lifetime.

The maximum sizes and lifetimes of the domain avalanches described here were not limited by finite-size

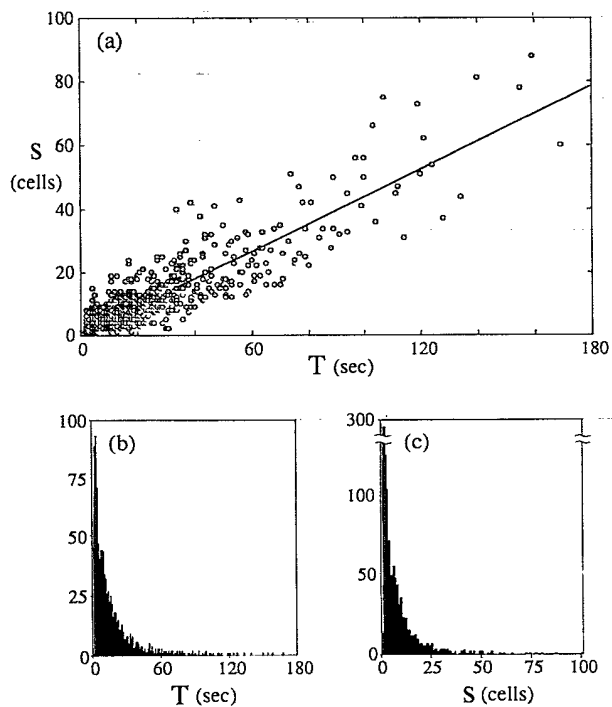


FIG. 2. (a) Avalanche size, determined as the number of cells eliminated, vs lifetime for 1105 avalanches. The line is an unweighted fit to the data, with slope  $0.43 \text{ sec}^{-1}$ . (b), (c) Histograms of avalanche lifetimes and sizes.

effects: The field of view used for our observations covered less than 4% of the usable, low-defect area of the garnet film. Nonetheless, arbitrarily large avalanches probably do not occur, because the destruction of cells tends to reduce stress in the pattern. The sizes of large avalanches are ultimately limited by the smooth and monotonically decreasing bias dependence of the average cell density  $n_c(H_B)$ , whose form is determined by the bias dependence of the stripe tension and the dependence of bubble-trap stability on local field.<sup>9</sup>

The avalanche size and lifetime distributions are shown in log-log plots in Figs. 3(a) and 3(b). To construct these plots, data for individual avalanches were logarithmically binned in  $s$  and  $T$ , and scaled to give the probability distributions  $D(T)$  and  $D(s)$  shown. Both distributions show tails which extend to large sizes and long lifetimes. As shown, these tails approximately follow power laws  $D(T) \propto T^{-2.3}$  and  $D(s) \propto s^{-2.5}$  over the last decade in  $s$  or  $T$ . A Poisson distribution with the

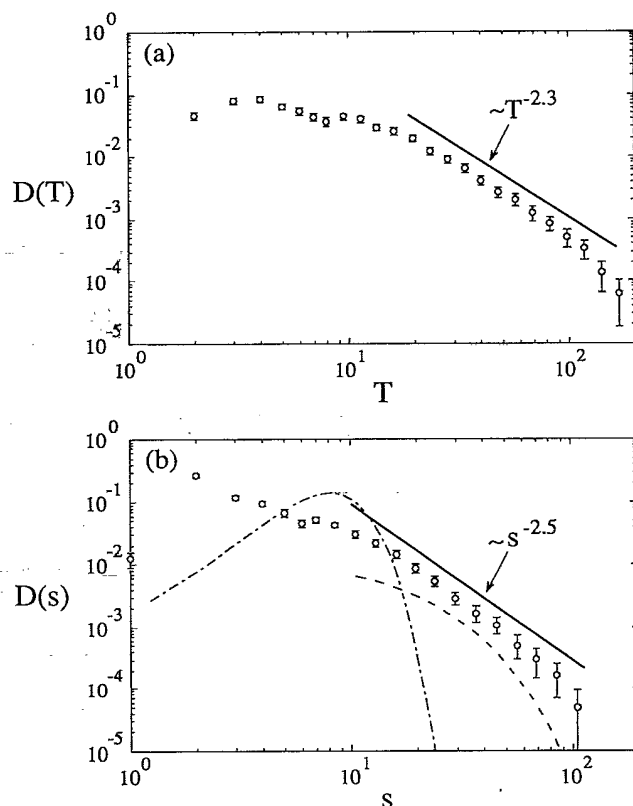


FIG. 3. Log-log plots of avalanche distributions obtained by logarithmically binning and averaging histogram data: (a) Distribution of avalanche lifetimes; the line shows a power law  $D(T) \propto T^{-2.3}$ . (b) Distribution of avalanche sizes; the line is a power law  $D(s) \propto s^{-2.5}$ . The dashed line is a best fit with an exponential distribution for sizes  $s > 10$  with characteristic size 12.3 cells, shifted downward slightly for clarity. The dash-dotted line is a Poisson distribution with the observed average  $\langle s \rangle = 8.5$  cells. The error bars represent  $[D/(\text{bin width})]^{1/2}$ .

measured average avalanche size (8.5 cells) is shown in Fig. 3(b) as the dash-dotted line; the data do not follow this standard distribution. An exponential distribution is another natural candidate, which might correspond to a "thermal" model in which the ac-field agitation creates an effective temperature. The dashed line in Fig. 3(b) is a best exponential fit to the data for  $s > 10$ , shifted down slightly for clarity. As shown, it is substantially more curved on a log-log plot than the data. It seems unlikely that a simple thermal model, or any other model in which cells are destroyed independently, would be appropriate, because domain avalanches occur as highly correlated chains of events connected by cell-wall motion.

Spatial disorder is necessary for the production of avalanches. We do not observe avalanches in ordered polycrystalline lattices of hexagonal cells, but rather a melting transition<sup>15</sup> that proceeds by the formation and propagation of a well-defined front that separates the lattice and a disordered cellular froth.

Simple models have been presented for the power spectra associated with self-organized criticality.<sup>3,6,16</sup> Within these models, we can estimate the power spectrum for the rate of cell elimination in domain avalanches that would occur if the bias field were increased slowly and continuously. The average rate of cell elimination  $s/T$  during an avalanche is approximately independent of the lifetime  $T$  (see Fig. 1). A linear superposition of rectangular pulses with constant height and duration  $T$  with the distribution  $D(T) \propto T^{-\alpha}$  leads<sup>16</sup> to a power spectrum  $S(f) \propto f^{-(3-\alpha)}$  for  $1 < \alpha < 3$ . The lifetime exponent  $\alpha \cong 2.3$  measured for domain avalanches would thus predict a  $1/f$  power spectrum for the rate of cell elimination:  $S(f) \propto f^{-0.7}$ . This spectrum relies on the assumptions of this simple model and is not a general result; other power laws may well occur in other systems.

In summary, we have found that nonequilibrium cellular magnetic-domain patterns undergo topological rearrangements with the character of avalanches. The avalanches produce barely stable patterns in a self-organizing manner over a substantial range of bias field,

bias increments, and average cell density. The distributions of avalanche size and lifetime span over 2 orders of magnitude and have long-time tails.

We are grateful to Roger Belt and the Airtron Division of Litton Industries for supplying the garnet sample, and Raj Seshadri for helpful conversations. This work was supported in part by the Office of Naval Research under Grants No. N00014-89-J-1023 and No. N00014-89-J-1592.

<sup>(a)</sup>Current address: Department of Physics, University of California, Santa Barbara, Santa Barbara, CA 93106.

<sup>1</sup>C. Tang *et al.*, Phys. Rev. Lett. **58**, 1161 (1987).

<sup>2</sup>J. M. Carlson and J. S. Langer, Phys. Rev. Lett. **62**, 2632 (1989).

<sup>3</sup>P. Bak, C. Tang, and K. Wiesenfeld, Phys. Rev. Lett. **59**, 381 (1987).

<sup>4</sup>These automata do not include some features of real sandpiles: For example, the static angle of repose can be larger than the dynamic angle of repose.

<sup>5</sup>X. Che and H. Suhl, Phys. Rev. Lett. **64**, 1670 (1990).

<sup>6</sup>P. Bak, C. Tang, and K. Wiesenfeld, Phys. Rev. A **38**, 364 (1988).

<sup>7</sup>R. F. Voss and J. Clarke, Phys. Rev. B **13**, 556 (1976).

<sup>8</sup>Recent experiments on real sandpiles found a narrowly peaked distribution of avalanche lifetimes [H. M. Jaeger, Chu-heng Liu, and Sidney R. Nagel, Phys. Rev. Lett. **62**, 40 (1989)].

<sup>9</sup>K. L. Babcock and R. M. Westervelt, Phys. Rev. A **40**, 2022 (1989).

<sup>10</sup>K. L. Babcock, R. Seshadri, and R. M. Westervelt, Phys. Rev. A **41**, 1952 (1990).

<sup>11</sup>K. L. Babcock, Ph.D. thesis, Harvard University, 1989 (unpublished), available from United Microfilms International, Ann Arbor, MI.

<sup>12</sup>R. F. Belt and J. B. Ings, Proc. SPIE **753**, 142 (1987).

<sup>13</sup>A. P. Malozemoff and J. C. Slonczewski, *Magnetic Domain Walls in Bubble Materials* (Academic, New York, 1979).

<sup>14</sup>D. Weaire and N. Rivier, Contemp. Phys. **25**, 59 (1984).

<sup>15</sup>K. L. Babcock and R. M. Westervelt, Phys. Rev. Lett. **63**, 175 (1989).

<sup>16</sup>H. J. Jensen, K. C. Christensen, and H. C. Fogedby, Phys. Rev. B **40**, 7425 (1989).